NetRAD: Monostatic and Bistatic Sea clutter Texture and Doppler Spectra Characterisation at S-Band

Matthew Ritchie, *Member*, *IEEE*, Andy Stove, *Senior Member*, Karl Woodbridge, *Senior Member*, *IEEE*, Hugh Griffiths, *Fellow*, *IEEE*

Electronic and Electrical Engineering Department, University College London, Torrington Place, London, WC1E 7JE

Abstract

This work describes the analysis performed on coherent, simultaneously recorded, monostatic and bistatic sea clutter data. The data were generated using a networked pulsed radar system, NetRAD. This analysis is completed in both the temporal and Doppler domains, and the parameters characterised are compared between multiple bistatic angles and different polarisations. The K-distribution model is used to assess the variation in the clutter amplitude statistics between multiple bistatic data and the corresponding monostatic data. Key characteristics of the Doppler data such as the spectrum width, centre of gravity and variance of the spectral width, are evaluated as a function of bistatic angle allowing novel relationships to be defined. The results conclude that the bistatic Doppler data has a lower K-distribution shape parameter in the majority of bistatic angles compared to the simultaneous monostatic data. In addition, novel trends in the relationship between the clutter spectrum center of gravity and the clutter intensity are presented.

1. Introduction

Recent radar research has shown a growing focus on the bistatic and multistatic properties of sea clutter. The potential advantages of networked coherent radar in detecting low observable targets within sea clutter has warranted experimental measurement campaigns aimed at quantifying the variations of the clutter as a function of the possible environmental, geometrical and RF sensor variables. With improved understanding of clutter diversity, it may be possible to deploy such systems to minimize the detrimental effects clutter has on the target detections.

This work presents the analysis of coherent sea clutter data recorded from NetRAD, which is a networked radar system with simultaneous monostatic and bistatic recording capabilities, [1-4]. Multiple datasets of monostatic and bistatic sea clutter recorded at varying fixed bistatic angles are characterised and

compared. The main focus of this work is the parameterisation of the clutter in the Doppler domain, along with the analysis of the additional parameters; temporal texture statistics and correlation. The quantifiable differences between the monostatic and bistatic clutter at multiple bistatic angles are then shown. This analysis represents a novel comprehensive comparison of simultaneous monostatic and bistatic sea clutter Doppler characteristics, at varying bistatic angles, with data obtained in both V and H polarisations.

Coherent sea clutter analysis is a critical area of maritime radar research. It is common within sea clutter analysis to assume a simple fixed Gaussian distribution for the Doppler structure of returned sea clutter echoes. However with increasing radar resolution and at lower grazing angles it has become clear that the empirically observed clutter behaviour departs significantly from this assumption. Early work by Pidgeon [5] looked to characterise the sea clutter as a function of Doppler frequency, this was then followed by Walker who presented a model which combined three Gaussian's to describe the Bragg, whitecap and sea-spike components of the spectra [6-7]. More contemporary analysis looked to evaluate the variation of the statistics of the clutter as a function of the Doppler frequency [8].

As the understanding of the behaviour of sea clutter with respect to Doppler has developed for the monostatic case, the added dimensions presented by bistatic or multi-static scenarios produce a challenge for radar research [9]. Little research has been completed into understanding simultaneous monostatic and bistatic sea clutter. Some recent modelling of the Normalized Radar Cross Section (NRCS) is reported in [10-11], as well as time domain amplitude statistical analysis with [12]. Even less prior research exists that quantifies the Doppler behaviour of simultaneous monostatic and bistatic sea clutter.

The analysis in this paper characterises of various parameters from both the temporal and Doppler domain components of each dataset. This is followed by the comparisons of these parameters between simultaneous monostatic and bistatic data, as well as across multiple bistatic angles and polarisations. The K-distribution model is utilised when evaluating the amplitude distributions and is described in more detail in Section 2. When applying the K-distribution modelling, the shape parameter is employed to characterise the statistical distribution of the intensity of the clutter return. In addition, the compound assumptions of this model were used to separate the rapid temporal decorrelation of the 'speckle' component, and the much slower decorrelation of the underlying gamma-distributed texture. The Doppler analysis is based on a

short-time Fourier transform model of the data, where each spectrum is taken over a period of the order of 128 ms. This time period is longer than the decorrelation time of the speckle but short enough to provide sufficient samples in the Doppler-time domain in order to perform statistical analysis. The changes in the shape (width) and position (centre of gravity) of the clutter spectra are compared from sample to sample and the decorrelation of the total clutter intensity is observed over the time scale of a large number of spectra. These parameters that were extracted from the time series and Doppler data have been selected from the same set defined within [13-14]. This allows for comparisons of the results shown within this work to prior research, as well as following a previously defined methodology that comprehensively quantifies the behaviour of sea clutter Doppler data.

The coherent spectra parameterisation of simultaneous monostatic and bistatic clutter across a range of bistatic angles and polarisations gives novel insight into the behaviour of bistatic clutter, therefore allowing the quantifying of potential advantages for multistatic radars in the maritime environment.

2. Theory

The theoretical basis of this research has been divided into two parts. Section 2.1 describes the sea clutter amplitude distribution theory; and Section 2.2 which describes the theory behind a previously defined sea clutter Doppler, the parameters contained within the model, and the methods used to extract the parameters.

2.1. Sea Clutter Distributions

Sea clutter amplitude distributions have been modelled by many theoretical distributions in the literature [15-16]. Distributions such as the log-normal [17], Weibull [18] and Pareto [19] have all been applied to various datasets of sea clutter. In this work, the key distribution used to model the amplitude distributions in time and Doppler has been the compound K-distribution, which was first applied to sea clutter within [20]. This has previously been shown to be a reliable fit to the amplitude distributions of sea clutter, both when observed with an incoherent radar [21] and to the distributions within the individual Doppler bins of a coherent radar [8]. In addition, this distribution has been shown to be a good fit to both

simultaneously generated bistatic and monostatic datasets [22-23], when the data is analysed in the time domain.

The K-distribution is the product of a gamma texture component modulated by a Rayleigh distributed speckle component. This two component distribution has been shown to fit empirically and, as mentioned previously, it allows different temporal and spatial decorrelation functions to be applied to these components. This is not possible when using some other models, but is a vital capability required for the model applied here.

The K-distribution PDF is

$$p(z) = \frac{2b^{\frac{\nu+1}{2}} z^{\frac{\nu-1}{2}}}{\Gamma(\nu)} K_{\nu-1}(2\sqrt{bz}) \quad (1)$$

where Γ is the gamma function, $K_{\nu-1}$ is the modified Bessel function of the second kind of order ν-1, *b* represents the scale parameter, and *ν* the shape parameter. It is the shape parameter that defines the length of the tail of the distribution.

The K-distribution can be compared to the real data via a Method of Moments (MoM) with the aim of characterising the closest theoretical representation for the data in each case. The moment estimated shape parameter, ν_{est}, is defined using the second order normalised moment, M_{N2}, see below,

$$\nu_{est} = \frac{1}{\frac{M_{N2}}{2} - 1} \quad (2)$$

The normalised 2nd order moments is defined as,

$$M_{N2} = \frac{\sum_{i=1}^{n} z_i^2 / n}{\bar{z}^2} \quad (3)$$

Where z is the intensity value of the clutter and $\bar{z}$ the mean values of the intensity. When fitting the shape parameter to the texture component of the clutter, which is Gamma distributed, this can also be estimated using MoM techniques. It is evaluated in the following way,

$$\nu_{est} = \frac{1}{M_{N2} - 1} \quad (4)$$

where M_{N2}, in this case, is the normalised second order moment of the texture component of the data. When considering the K + Noise distribution case, [24] the shape parameter MoM estimate value becomes,

$$\nu_{K+Nest} = \frac{2(M_1 - P_N)^2}{M_2 - 2M_1^2} \quad (5)$$

Where M_1 and M_2 are the un-normalised first and second order moments respectively and P_n represents the thermal noise power within the signal.

We have used equation (5) to estimate the shape parameter in cases where the clutter to noise ratio is between 3dB and 12dB. At higher clutter to noise ratios the simpler equation (4) is adequate and at lower levels the clutter levels are so low that it's better to assume that we are just seeing the noise background.

In this paper the K-distribution is fitted to sea clutter amplitude values within both the temporal and Doppler domains. For the case of the temporal components of the clutter, the Gamma texture element has been fitted using MoM, and for the Doppler domain case, the K-distribution was fitted within each Doppler bin. In each case, this allows for a quantitative comparison in the shape parameters between simultaneous monostatic and bistatic clutter, as well as the underlying trends seen with varying bistatic angle.

2.2. Sea Clutter Doppler Spectra Model

The time domain data has been parameterised by the temporal correlation and Gamma shape parameter of the texture component. The texture component of sea clutter has been shown to possess temporal correlation over a period of several seconds, in comparison to the speckle components decorrelation time, which is approximately 10 ms at X-band [15], and so would be expected to be about 40 ms at 2.4 GHz. By applying a block average of 128 samples in length, on the raw time series data, it is possible to reduce the effect of the speckle component within the data, thus focusing the analysis on the temporal correlation of the texture, in addition to this when characterising the average correlation of the texture component with the data averaging over numerous range bins ensures that overall trends of texture correlation are modelled. MoMs were applied in order to obtain the Gamma shape parameter of this block averaged data.

The correlation properties of the texture component of the clutter were quantified using an Autocorrelation Function (ACF). For the purpose of this analysis, the ACF is defined as,

$$ACF_Z(j) = \frac{1}{z}\sum_{n=0}^{Z-1}(x(n) - \bar{x})(x(n-j) - \bar{x}) \quad (6)$$

$ACF_N(j)$ is the Autocorrelation function of the signal at lag j, $x(n)$ is nth sample of the block averaged time samples of clutter data, $\bar{x}$ is the sample mean of the data, Z is the length of the signal. The autocorrelation coefficient has been used to define the correlation of the data in the time domain from the intensity values within individual range gates, which is defined as $ACF_Z(j) / ACF_Z(0)$.

As well as characterising the clutter present in both monostatic and bistatic data when observed incoherently, the Doppler spectra will be modelled for both types of geometry. The modelling methodology used was first defined in [13]. This uses a Gaussian shaped power spectral density (PSD), which follows the type of behaviour noted in [6-7]. The Gaussian based PSD is defined by,

$$G(f,x,s) = \frac{x}{\sqrt{2\pi}s}\exp[-\frac{\left(f-m_f(x)\right)^2}{2s^2}] \quad (7)$$

where x is the texture intensity, f is the Doppler frequency, $m_f(x)$ is the mean Doppler frequency and s is the spectrum half width (standard deviation of Gaussian spectrum).

The centre of gravity of the PSD, $m_f(x)$, was the first parameter to be extracted from the data. Within this analysis the $m_f(x)$ is defined as the centre of gravity (CoG) of a given spectrum which is defined as,

$$CoG = \sum_{i=1}^{N} \frac{PSD_i.F_i}{PSD_i} \quad (8)$$

where F_i is the frequency of the Doppler bin, N is the number of Doppler bins and PSD_i is the amplitude value of the data PSD in Doppler bin i. Alternative methods can be used to define the $m_f(x)$ values for the model, such as the peak value, but for this analysis the CoG was found to be effective. It is assumed that the CoG is linearly related to the intensity of a given PSD. This linear relationship was fitted to extracted parameter values using a least square fitting technique.

The parameter related to the PSD half width values, s, is defined as a random normally distributed variate that has a mean and variance that can be estimated directly from the data. The representative sigma values for each data PSD were obtained by evaluating the full widths of the PSD at -3 dB and -5 dB points from the peak and then relating this to the half width sigma value. The average of the two PSD widths were used to increase the accuracy of the representative Gaussian shape. The sigma values are defined using the relationship of the width, Δx, at -3 dB and -5 dB from the peak are:

$$\sigma_{3dB} = \frac{\Delta x}{2\sqrt{2.\ln(2)}} \tag{9}$$

$$\sigma_{5dB} = \frac{\Delta x}{2\sqrt{2.\ln(\sqrt{10})}} \tag{10}$$

The mean sigma values from each range gate of data have been defined and are compared between datasets in Section 4.2.

3. Radar system and Data

The data used in this analysis were generated using the University College London (UCL) radar system, NetRAD. This system is a multi-node, wirelessly networked, pulsed radar. It operates in the WiFi ISM band centered on 2.4 GHz, while using wireless data links at 5.8 GHz to network all three nodes. GPS disciplined oscillators (GPSDOs) that have been developed by the University of Cape Town are used to synchronize the nodes both in time and frequency [25-26]. The properties of the system can be seen in Table 1.

The data was recorded during a series of trials commencing in October 2010 on the coast of South Africa near the Cape Point area. The radar was set up using a baseline that ran northwest to southeast. The grid reference for the locations were 34°10’36.39’’ S 18°21’11.9’’ E for the monostatic node and 34°11’20.66’’ S 18°21’59.33’’ E for the bistatic node. These locations gave a baseline separation between the two nodes of approximately 1830 m and the bearing from transmitter to bistatic receiver was approximately 138°. The wind was northerly, i.e. its velocity vector was along a bearing of approximately 180°.

During the trials the azimuth angles of both the monostatic and bistatic nodes were simultaneously altered to create a new geometry generating the desired bistatic angle β, see in Fig. 1. Three bistatic angles have been used for analysis, 60°, 90° and 120°. The sea clutter measurements from all bistatic angles were measured using both Horizontal (HH) and Vertical (VV) co-polarisation sequentially. This resulted in an array of 6 different measurements from both the monostatic and bistatic nodes. Due to the method of obtaining new bistatic angles, the location of the patch of sea that is illuminated varied. The distance of the intersection point from the baseline for bistatic angles 60°, 90° and 120° is 1585 m, 915 m and 528 m

respectively. The two-way bistatic range of the data used from each bistatic angle is shown within Table. 2. For the comparison of the data and statistics, the variation due to this change in geometry is assumed to be of reduced significance in comparison to the changes introduced by the bistatic scattering behaviour. Over this change in range the grazing angle varies from approximately 0.6° to 1.5°, which is a relatively small variation in angle ensuring the data is all within the domain of low grazing angle geometries. Variations in the clutter cell size, range and grazing angle are all present between the selected datasets. The analysis presented here attempts to evaluate the key trends in modelling parameters and emphasizes differences between simultaneous monostatic and bistatic results as direct comparisons can be made from these datasets. The range gates of interest have been defined and the data parameterisation was limited to these range gates. The key factor that limits the range gates that are of interest, is the location of the intersection clutter patch in the bistatic data. The patch varies in size and location as the bistatic angle is changed.

The meteorological information on wind and wave parameters can be seen in Table. 3. Overall, the conditions were relatively stable over the timescale of collecting the 6 datasets, with a reasonably small variation of 0.7 m in wave height and 2 ms^{-1} in wind speed. This makes direct comparisons between experiments more relevant, as the changes are dominated by the bistatic angle change or polarisation, not changing sea or wind conditions. The significant wave height ($H_{1/3}$) corresponds to a Douglas and World Meteorological Organisation sea state of 3.

4. Sea Clutter Data Analysis

The parameters of the data that have been analysed are the following:

1. Texture parameters
    a. Gamma shape parameter
    b. Temporal Correlation
2. Doppler Spectra parameters
    a. Mean Spectra Width
    b. Variance of Spectra Width
    c. Spectra Centre of gravity

d. Linear relationship between intensity and centre of gravity

e. Clutter-to-Noise (dB)

The majority of the listed parameters were selected to be the same as those shown in [13]. The characteristics of each of these parameters, and how they vary with bistatic angle, range, or polarisation, is discussed and compared in the following sections.

4.1. Texture parameters

Texture Gamma Shape Parameter

As described in Section 2.1 the amplitude characteristics of the texture component of sea clutter can be evaluated using MoM; using the Gamma shape parameter Eqn. (4). These moments have been evaluated using the normalised power time samples over the range gates of interest. Each range gate was block averaged with a sliding window of length 128. This processing step was completed to reduce the influence of the speckle components of the clutter, leaving the dominant gamma texture component. The length of the window was selected to be 128 consecutive samples with a PRF of 1 kHz (128 ms in time) as this was found to be sufficiently long in comparison to the speckle decorrelation time, which has been defined as being of the order of 10 ms for X-band clutter, [15].

Table 4 shows the average value of the MoM fitted Gamma shape parameters of the texture component of the clutter. The shape parameters were evaluated for each range gate and then the average values over all range gates of interest for each dataset, see Table 2. The monostatic V polarisation data has a greater Gamma shape parameter in comparison to those found for the H polarisation data. This agrees with prior literature, which states that H polarised data is more spikey, and hence would have a smaller shape parameter [15]. The bistatic data shows a significant difference between the H and V polarised values, the H pol shape parameters are shown to monotonically increase with bistatic angle, whereas the V pol values reduce from $\beta = 60°$ to 90° but then increase from $\beta = 90°$ to 120°, shown clearly in Fig. 2. In all cases, except for V pol $\beta = 60°$, the bistatic Gamma distribution shape parameter is found to be greater than the equivalent monostatic result. This difference is found to be greatest within the H pol texture results.

These results quantitatively shows that, on average, the monostatic data has a longer tailed distribution representing the texture component, compared to the equivalent simultaneous bistatic data.

Texture correlation

The temporal autocorrelation for the time series texture samples within each range gate from all datasets has been evaluated. The correlation was obtained using Fourier analysis techniques on the same block averaged time samples that were previously used to evaluate the texture shape parameter. The correlation was then averaged over the range gates of interest within each dataset. The averaged ACF from each bistatic angle for horizontally and vertically polarised data are plotted in Fig. 3 and 4 respectively.

It is clear that for the H polarised data there is very little long-term correlation in the averaged monostatic data. The H bistatic data does show some long-term periodic correlation in the $\beta = 90°$ and 120° datasets. In the V polarisation data the long-term correlation is much clearer within both monostatic and bistatic for $\beta = 60°$, and more predominately seen in the bistatic data form $\beta = 90°$ and 120°. It is worth noting that the monostatic and bistatic ACF is most closely matched for the V polarisation $\beta = 60°$ case, whereas for the $\beta = 90°$ and 120° case the bistatic and monostatic ACF vary significantly.

4.2. Doppler parameters

Centre of gravity

The averaged CoG for each PSD as a function of range gate has been plotted from all the datasets in Fig. 5 and 6 for the horizontally and vertically polarised data respectively. These values were defined using 10 block averaged consecutive Doppler PSDs. The block averaged PSDs were then interpolated in Doppler, by a factor of 10, using a spline interpolation methodology in order to increase the number of Doppler samples from 64 to 640. The CoG values have been plotted against the two-way range, which varies with the intersection patch for each bistatic angle. The bistatic angle $\beta = 60°$ has the greatest distance to the intersection patch while $\beta = 120°$ has the shortest distance, see Table 2.

The H polarised data shows a trend of increasing CoG with range for the bistatic data at $\beta = 120°$ and 90°. While the bistatic data at $\beta = 60°$ shows a decrease in the CoG value with range. This implies that

there is a point of inflection in the increasing to decreasing CoG trend which exists at approximately 3000 m two-way range and a bistatic angle between 60° and 90°.

The monostatic data at β = 60° demonstrates the same approximate gradient in decreasing CoG with range as the bistatic equivalent. At bistatic angles β = 120° and 90° the monostatic data does not echo the same gradient of change in CoG with range compared to bistatic data, with the β = 120° having a negative gradient and the β = 90° a positive one. The H polarised data shows little variance between samples as a function of range and the bistatic and monostatic data at β = 120° is shown to have the least variance (smoothest curve).

The V polarised data in the monostatic case does not extend to the same negative Doppler CoG values that the H polarised data reduced to, across all β angles. The difference between monostatic and bistatic values ranges between 5-15 Hz for all β values. The mean values shown for the β = 90° bistatic case demonstrate a very large variance between the samples. The variance in these fitted values is unlike the trends seen in all of the other datasets; it is unknown what phenomena is causing this. In further analysis it is important to be aware that this dataset is showing odd behaviour. Due to this variance it is difficult to assess whether the V polarised data also has the increase in CoG trend seen in the bistatic β = 120° and 90° datasets that was shown with in the H polarised data. The decrease of CoG in the β = 60° result is present for the V data, as was shown in the H polarised case, but the corresponding monostatic CoG variation is flat with range compared to the bistatic data. The averaged CoG value across all range gates in each dataset can be seen in Table 5.

Mean and variance of PSD Width

The mean PSD sigma values were defined using the same block averaged and interpolated PSD data that was used when evaluating the CoG values of the PSD. These have been plotted as a function of range gate for each Bistatic angle from the horizontal and vertical polarised dataset in Fig. 7 and 8 respectively. The values plotted are the averaged fitted values for sigma, defined in Eqn. (9) and (10). The closest agreement in mean PSD sigma value between monostatic and bistatic data is shown at β = 60°, while the H data at β = 120° shows the greatest separation. For the V dataset at β = 90° a significant variance is shown

in the mean PSD sigma, which matches with the increased variance seen in the CoG results in Fig. 6. The trends seen in these results will be strongly dependent on the geometry of the system with respect to the wave and wind direction. All the averaged mean PSD sigma values can be seen in Table. 6 for both H and V polarised data.

Intensity vs. Centre of Gravity

A linear fit was applied, using a least square fitting technique. This defines the relationship between the CoG for each PSD and the intensity for a given dataset. This was completed on each PSD within all range gates of the data. The parameters of the fit were defined as:

$$M_f = A + B.x \tag{11}$$

where M_f is linear fit, *A* is the offset and *B* is the gradient of the fit. The mean values for parameters *A* and *B* are plotted against each other for each dataset for the H and V data within Fig. 9 and 10 respectively.

The datasets are shown to consistently have a *B* parameter that decreases with increasing bistatic angle. The bistatic results yield greater values than the equivalent monostatic result for both V and H polarisation. In both the V and H polarised results, the *B* values for the $\beta = 60°$ and 90° case were much closer spaced than the $\beta = 120°$, possibly indicating that a step change has occurred in the overall trend in CoG. Along the *A* axis it was shown that the monostatic and bistatic data has separate groupings, which represents the different offset values from the negative and positively shifted PSDs in each case. A comparison of the variance of the *A* shows that for the H case, the bistatic values have a greater variance, 5.8 compared to 2.2, while for the V data the bistatic data has a significantly reduced variance, 0.4 compared to 1.2.

Clutter to Noise Ratio

The noise level within the data was evaluated using selected range gates that were noise limited within the monostatic and bistatic data. The mean CNR levels within the dataset were evaluated for each

range gate. The average CNR levels across all range gates of interest, which were defined in Table. 2, are shown within Table. 6.

The CNR values for all datasets are above 6 dB's, ensuring that there was sufficient clutter present in all the data analysed. The monostatic CNR values are greater than the equivalent bistatic values, with the exception of the $\beta = 120°$ H polarised result. The V polarised CNR levels are shown to be greater than the corresponding horizontal polarisation values in all cases. The most significant differences between monostatic and bistatic CNR values are shown within the V datasets at $\beta = 60°$ and 90°, whereas the H datasets show more comparable levels between monostatic and bistatic.

K-distribution Shape Parameter vs. Doppler

The variation of amplitude statistics with Doppler bin is a vital characteristic of the sea clutter. It helps define the behaviour of the clutter across its spectra, and gives information regarding the adaptive thresholding that would be required to ensure the operation of a Constant False Alarm Rate (CFAR) detector in the Doppler domain.

The amplitude statistics of the time samples, within each Doppler bin, from the spectrogram processed data were used to estimate the K and K+Noise distribution shape parameters using Eqn (2) and (5). A hybrid representation of the shape parameter is shown in the resulting data which selects either the K or the K+Noise distribution parameter depending on the CNR of the Doppler bin. The shape parameter was evaluated for each range bin and then the average value was used to define the variation with Doppler. The K-distribution shape parameters were used when the Doppler bin average CNR was found to be below 3 dB and above 12 dB, for CNR between these two values a K+Noise shape parameter was used. The CNR levels above 12 dB are defined as the endo-clutter region located centrally within the main clutter peak, while the CNR levels below 3 dB were found in the noise dominated exo-clutter sections of the data.

The results for the H and V datasets can be seen in Fig. 11 and 12 respectively. This has been plotted as an inverse shape parameter to present the variations in obtained values more clearly. In each case the upper graph is the monostatic data and the lower is the bistatic.

The H statistics are shown to have a clear double peak in the inverse shape parameter for the β = 60° and 90° monostatic datasets, which was previously reported within [23]. For the β = 120° case the shape parameter variation is dominated by a single peak at approximately -100 Hz. A second smaller peak is present at 25 Hz, but this is much reduced compared to the peak at the same frequency within the β = 60° and 90° datasets. The bistatic data shows a single peak structure for all bistatic angles. This peak is shown to reduce with bistatic angle, most significantly for the β = 120° case. A secondary raised section is present between -175 Hz and -50 Hz for the bistatic data, but it does not show the same clear peaked form seen in the monostatic results.

For the V data the inverse shape parameters were shown to be smaller in comparison to the H datasets, which agrees with the prior literature on the comparison of Doppler statistics between different polarized sea clutter data [15]. For bistatic angles 90° and 120° the monostatic is seen to have a greater peak inverse shape parameter than the bistatic, while the opposite is true for the β = 60° case. The monostatic data only exhibits a clear double peaked structure for β = 60°, for β = 90° and 120° the inverse shape parameter appears to have only a single peak, consistently seen at -75 Hz. The bistatic results all show a single peak, although these peaks are shifted relative to the monostatic case. In the β = 90° there is an increase in the inverse shape parameter between -125 Hz and -175 Hz. It is thought that unwanted targets within the beam may have caused this, as it is a significant Doppler velocities that are unlikely to be due to the sea clutter. The vertically-polarised bistatic data at β = 90° and β = 120° (i.e. closer to the shore) shows a long 'tail' at low amplitude covering positive Doppler shifts up to the ambiguous velocity, which corresponds approximately to the wind speed of about 10 ms^{-1}, but does not extend beyond the ambiguous speed. This may be due to wind-blown spray, which would be driven by the local breeze blowing from sea to shore.

5. Conclusion

This paper has comprehensively analysed and compared multiple features of simultaneous monostatic and bistatic sea clutter data, in both the time and Doppler domain. The comparisons at each stage have presented quantitative values demonstrating the different behaviours of the monostatic and bistatic sea clutter data, as a function of bistatic angle and polarisation.

A clear relationship in the fitted linear parameters of the PSD CoG against intensity was shown. The gradient variable *B* was shown to decrease as a function of increasing bistatic angle for both polarisations and in both the monostatic and bistatic cases. These results will be geometry dependent, in relation to the wind and wave direction; therefore further experimental data is required to investigate these trends.

A clear variation in texture shape parameter has been shown within the analysis of the data. A linear relationship between the texture Gamma shape parameter was seen in the V polarised data, while in the H polarised case a dip in the $\beta = 90°$ data demonstrated a different behavior. In previous literature the K-distribution shape parameter has been shown to be more dependent on swell than wind direction [27]. When comparing the monostatic and bistatic variation in shape parameter the change in look angle with respect to wind and swell direction must be taken into account.

The key conclusions of this analysis are that the bistatic clutter is shown to have a reduced peak in inverse k-distribution shape parameter as a function of Doppler in both the H and V polarised data for bistatic angles 90° and 120°, while at 60° the opposite was shown. There is a trend to see a double peaked structure within the monostatic inverse shape parameter while on average, the bistatic data shows only single peak. This has significant potential as using Doppler CFAR detection methodology allows for reduced thresholds and increased sensitivity to low observable targets when using a bistatic radar.

Acknowledgments

The authors would like to thank the team at University College London and the University of Cape Town who collected the data, with particular thanks going to Dr. Waddah Al-Ashwal, Stephan Sandenbergh, Prof. Simon Watts and Prof. Mike Inggs. The development of the NetRAD system and the experimental campaign were funded by Thales UK, Thales Netherlands, US Office of Naval Research (Global) and the University of Cape Town. This analysis of data is funded by the Engineering and Physical Sciences Research Council (EPSRC).

References

[1] T. Derham, S. Doughty, K. Woodbridge, and C. Baker, “Design and evaluation of a low-cost multistatic netted radar system,” *Radar, Sonar Navigation, IET*, vol. 1, no. 5, pp. 362 –368, Oct. 2007.

[2] T. Derham, S. Doughty, K. Woodbridge, and C. J. Baker, “Realisation and evaluation of a low cost netted radar system,” *Proceedings CIE International Conference on Radar*, 2006.

[3] M. Inggs, G. Inggs, S. Sandenbergh, W. Al-Ashwal, K. Woodbridge, and H. Griffiths, Multistatic networked radar for sea clutter measurements," *in IEEE International Geoscience and Remote Sensing Symposium (IGARSS)*, 2011.

[4] W. A. Al-Ashwal, “Measurement and modelling of bistatic sea clutter," Ph.D. dissertation, University College London, UK, 2011.

[5] W. Pidgeon, “Doppler Dependence of Radar Sea Return,” *Journal of Geophysical Research*, vol. 73, no. 4, 1968.

[6] D. Walker, “Experimentally motivated model for low grazing angle radar Doppler spectra of the sea surface,” *IEE Proceedings Radar, Sonar and Navigation*, vol. 147, no. 3, pp. 114 –120, June 2000.

[7] D. Walker, “Doppler modelling of radar sea clutter,” *IEE Proceedings Radar, Sonar and Navigation*, vol. 148, no. 2, pp. 73 –80, April 2001.

[8] M. A. Ritchie, K. Woodbridge, and A. G. Stove, “Analysis of sea clutter distribution variation with Doppler using the compound k-distribution,” in *Proceedings IEEE Radar Conference*, Washington D.C, 2010, pp. 495–499.

[9] S. Watts, “Radar sea clutter: recent progress and future challenges,” *in Proceedings International Radar Conference*, 2008, pp. 10–16.

[10] H. Griffiths, W. A. Al-Ashwal, K. Ward, R. Tough, C. Baker, and K. Woodbridge, “Measurement and modelling of bistatic radar sea clutter,” *IET Radar, Sonar and Navigation*, vol. 4, no. 2, pp. 280–292, 2010.

[11] W. A. Al-Ashwal, K. Woodbridge, and H. D. Griffiths, "Analysis of bistatic sea clutter Part I: Average reflectivity," *IEEE Transactions on Aerospace and Electronic Systems*, vol. 50, pp. 1283-1292, 2014.

[12] W. A. Al-Ashwal, K. Woodbridge, and H. D. Griffiths, "Analysis of bistatic sea clutter Part II: Amplitude statistics," *IEEE Transactions on Aerospace and Electronic Systems*, vol. 50, pp. 1293-1303, 2014.

[13] S. Watts, “A new method for the simulation of coherent sea clutter,” *in IEEE Radar Conference*, pp. 52 -57, May 2011.

[14] S. Watts, “Modeling and simulation of coherent sea clutter," *IEEE Transactions on Aerospace and Electronic Systems*, vol. 48, no. 4, pp. 3303-3317, 2012.

[14] G. Davidson, “Simulation of coherent clutter,” *IET Seminar on Radar Clutter Modelling*, pp. 33–39, 2008.

[15] K. D. Ward, R. J. Tough, and S. Watts, “Sea Clutter: Scattering, the K Distribution and Radar Performance,” *IET Radar Sonar and Navigation*. London, 2006.

[16] M. Greco, F. Gini, and M. Rangaswamy, “Statistical analysis of measured polarimetric clutter data at different range resolutions,” *IET Proceedings Radar, Sonar and Navigation*, vol. 153, no. 6, 2006.

[17] G. V. Trunk and S. F. George, "Detection of Targets in Non-Gaussian Sea Clutter," *IEEE Transactions on Aerospace and Electronic Systems*, vol. AES-6, pp. 620-628, 1970.

[18] D. C. Schleher, "Radar Detection in Weibull Clutter," *IEEE Transactions on Aerospace and Electronic Systems*, vol. AES-12, pp. 736-743, 1976.

[19] G. V. Weinberg, "Assessing Pareto fit to high-resolution high-grazing-angle sea clutter," *Electronics Letters*, vol. 47, pp. 516-517, 2011.

[20] K. D. Ward, "Compound representation of high resolution sea clutter," in Electronics Letters, vol. 17, no. 16, pp. 561-563, August 6 1981.

[21] A. Farina, F. Gini, M. Greco, and L. Verrazzani, “High resolution sea clutter data: statistical analysis of recorded live data,” *IEE Proc. Radar, Sonar and Navigation*, vol. 144, no. 3, p. 121, 1997.

[22] W. A. Al-Ashwal, C. J. Baker, A. Balleri, H. D. Griffiths, R. Harmanny, M. Inggs, W. J. Miceli, M. A. Ritchie, J. S. Sandenbergh, A. G. Stove, R. J. A. Tough, K. D. Ward, S. Watts, and K. Woodbridge, “Statistical analysis of simultaneous monostatic and bistatic sea clutter at low grazing angles,” *Electronics Letters*, vol. 47, no. 10, pp. 621–622, 2011.

[23] M. A. Ritchie, W. Al-Ashwal, A. Stove, K. Woodbridge, and H. Griffiths, “Statistical analysis of monostatic and bistatic sea clutter Doppler spectrum,” *in Proceedings CIE International Conference on Radar*, pp. 816–820, Oct. 2011.

[24] S. Watts, "Radar Detection Prediction in K-Distributed Sea Clutter and Thermal Noise," *IEEE Transactions on Aerospace and Electronic Systems*, vol. AES-23, pp. 40-45, 1987.

[25] J. S. Sandenbergh and M. R. Inggs, "A common view GPSDO to synchronize netted radar," *IET International Conference on Radar Systems*, pp. 1-5, Oct 15-18, Edinburgh. 2007

[26] J. S. Sandenbergh, M. R. Inggs, and W.A.Al-Ashwal, “Evaluation of coherent netted radar carrier stability while synchronised with GPS-disciplined oscillators”, *IEEE Radar Conference*, pp. 1100-1105, May 23-27, Kansas City, 2011.

[27] D. Crisp, L. Rosenberg, N. Stacy, and Y. Dong, “Modelling x-band sea clutter with the k-distribution: Shape parameter variation,” *in Proceedings SEE International Radar Conference*, pp. 1 –6, Oct. 2009.

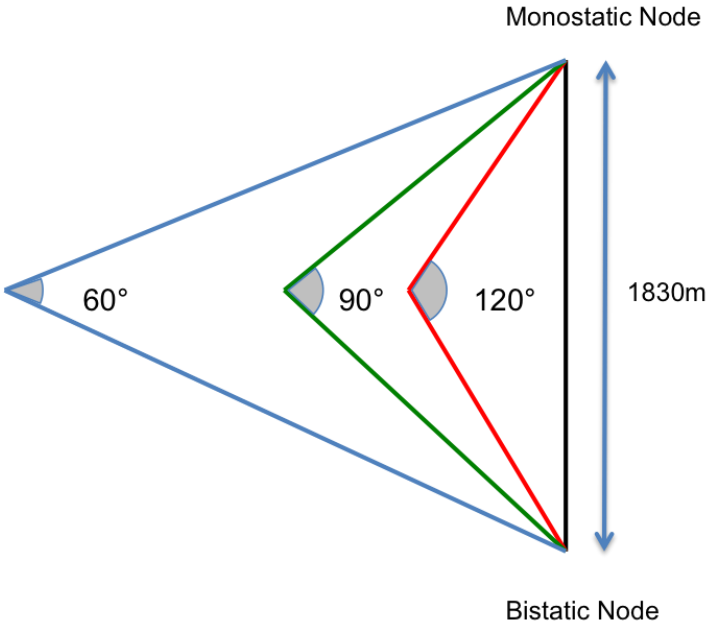

Figure 1 NetRAD Measurement geometry [4]

Table 1 Summary of the datasets with bistatic angle and polarization

Parameter	**Value**
Central Frequency	2.45 GHz
Bandwidth	45 MHz
Peak Transmit Power	57.7 dBm
Monostatic Range Resolution	4.9 m
PRF	1 kHz
Pulse Lengths	0.4-20 μs
Polarisation	HH and VV
Antenna Beamwidth	11.3° in E-plane and 8.9° in H-plane
Antenna Gain	23.8 dBi

Table 2 Ranges of interest

Bistatic Angle (°)	Two-Way Range of interest (m)
60	3228 - 4002
90	2310 - 2826
120	1962 - 2304

Table 3 Meteorological Conditions

Bistatic Angle (°)	Pol	Wind speed (ms^{-1})	Wave Period (s)	Wave direction (°)	$H_{1/3}$ (m)
60	V	10.15	7.1	289	3.28
90	V	10.37	7.7	279.5	3.48
120	V	10.8	8.3	270	3.67
60	H	11.55	8.3	283	3.89
90	H	11.55	8.3	283	3.89
120	H	12.3	8.65	276	4.02

Table 4 Average value of MoM fitted Gamma Shape parameter of Clutter Texture

Bistatic Angle (°)	Polarisation			
	H		V	
	Mono	Bi	Mono	Bi
60	0.20	0.32	1.03	0.80
90	0.38	3.6	0.48	2.51
120	0.19	5.90	1.96	2.01

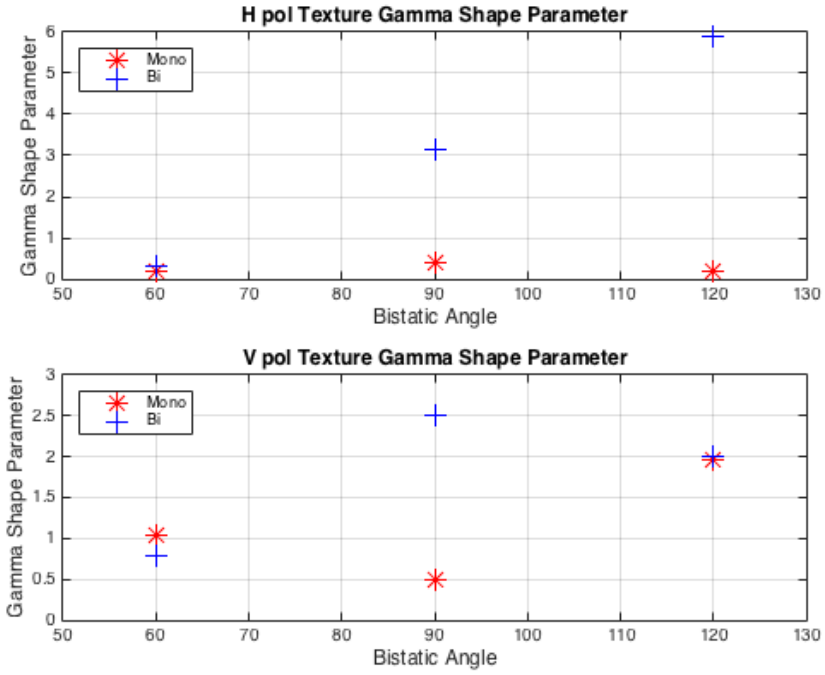

Figure 2 H and V pol Texture Gamma shape parameter plotted against bistatic angle

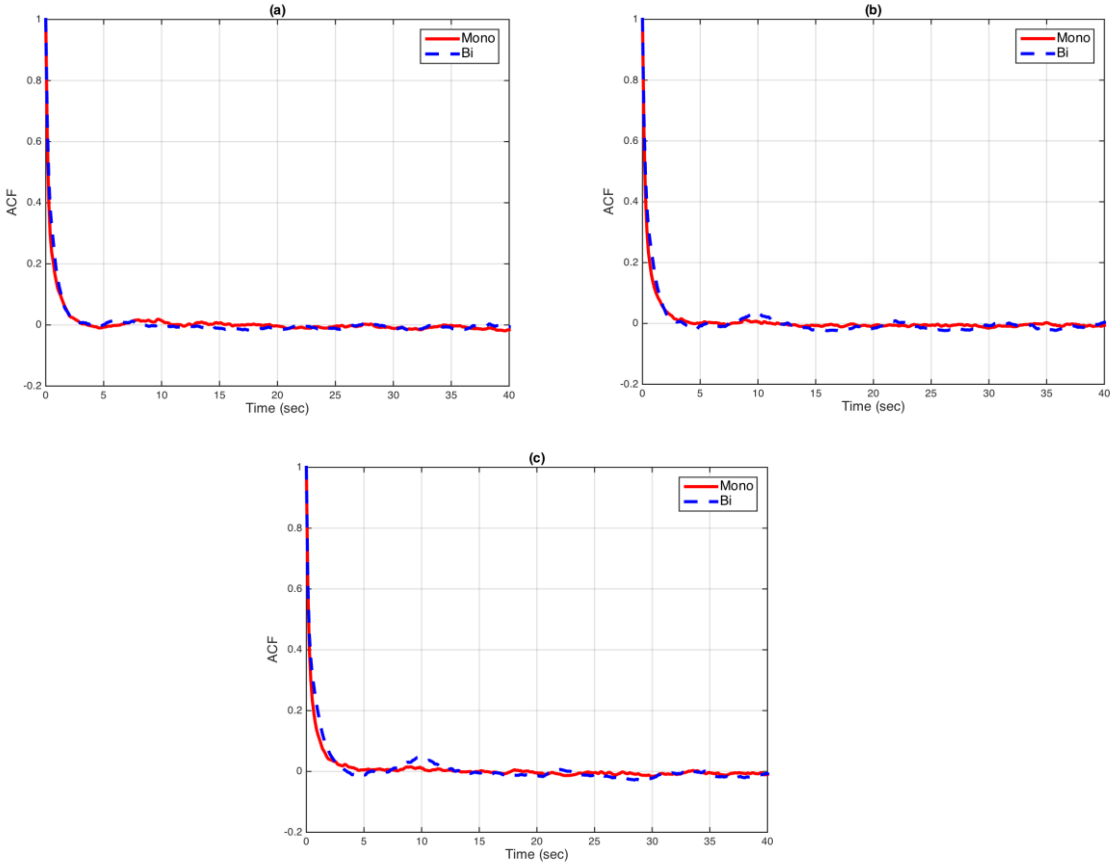

Figure 3 ACF for Horizontal Polarised Data at (a) β = 60° (b) β = 90° (c) β =120°

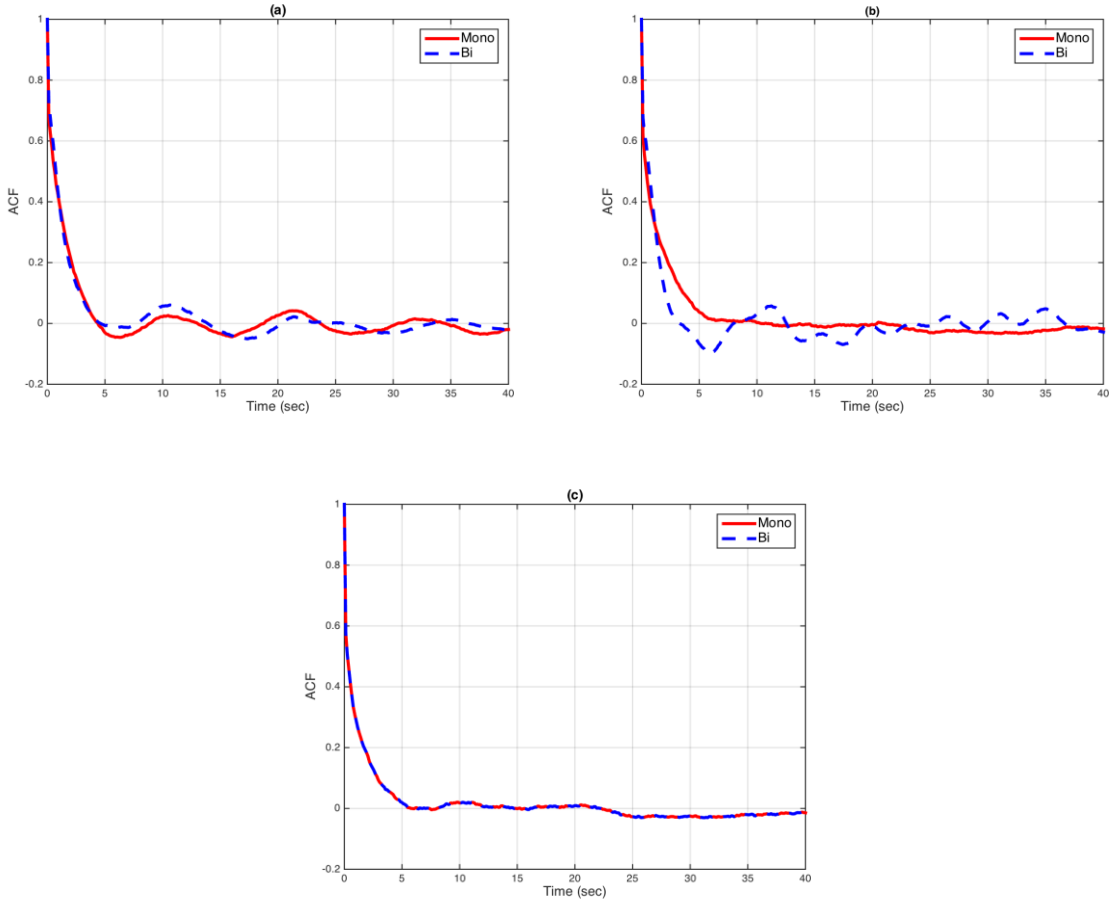

Figure 4 ACF for Vertical Polarised Data at (a) β = 60° (b) β = 90° (c) β =120°

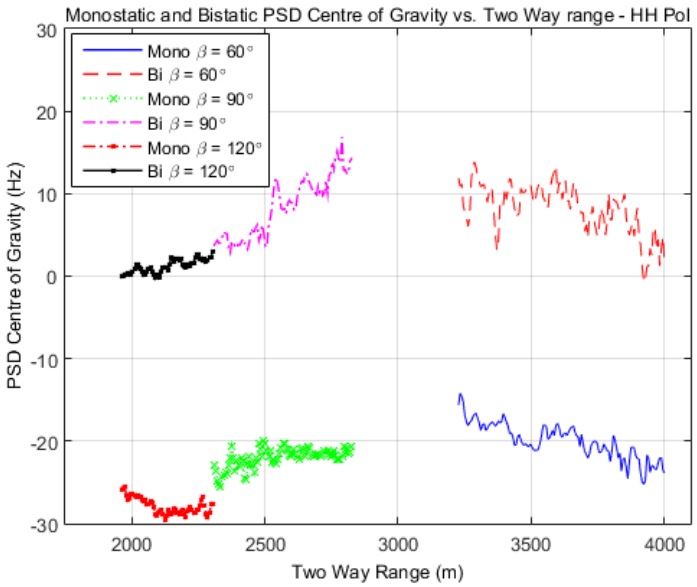

Figure 5 Monostatic and Bistatic PSD Centre of Gravity vs. Two way Range for Horizontal Polarisation

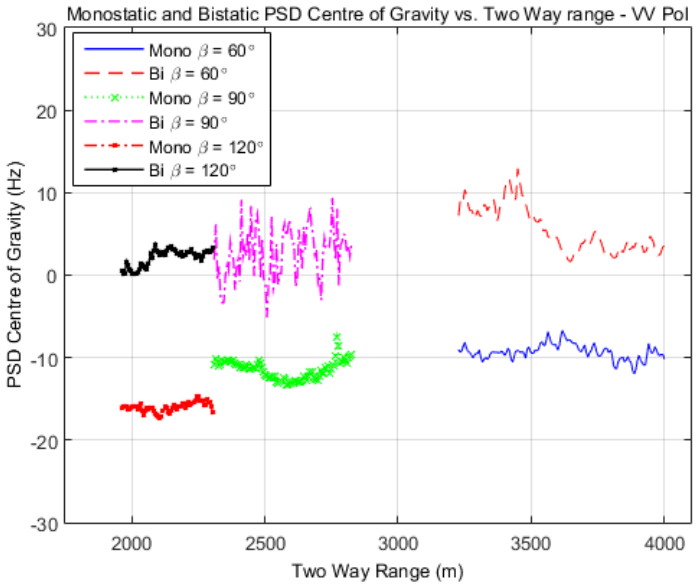

Figure 6 Monostatic and Bistatic PSD Centre of Gravity vs. Two way Range for Vertical Polarisation

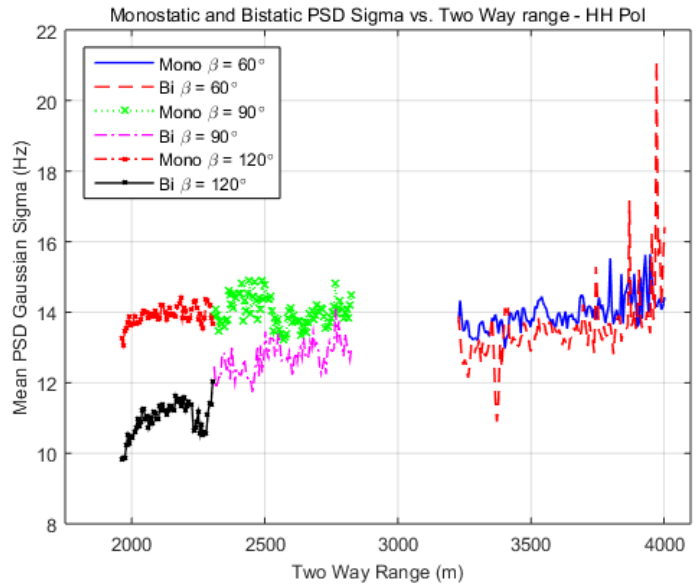

Figure 7 Monostatic and Bistatic PSD Sigma vs. Two way Range for Horizontal Polarisation

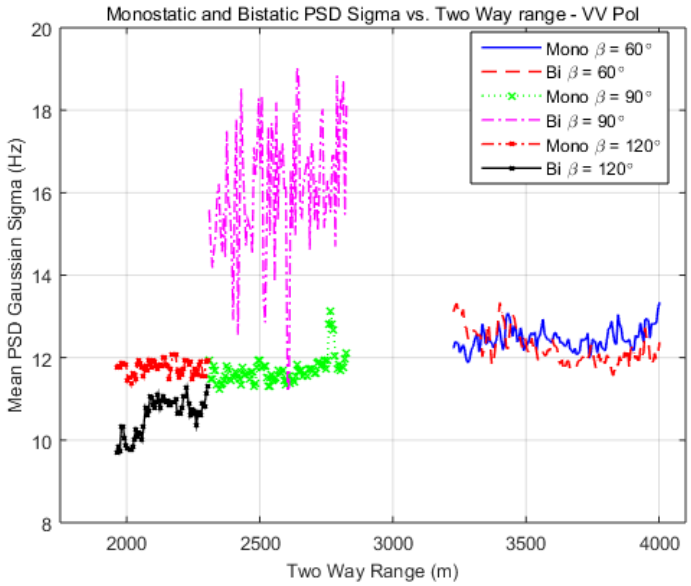

Figure 8 Monostatic and Bistatic PSD Sigma vs. Two way Range for Vertical Polarisation

Table 5 Range Averaged Mean PSD Gaussian width sigma and Centre of Gravity

Bistatic Angle (°)	Horizontal Polarisation			
	Mono		Bi	
	Sigma (Hz)	CoG (Hz)	Sigma (Hz)	CoG (Hz)
60	13.98	-19.96	13.54	8.20
90	14.01	-22.01	12.72	8.39
120	13.90	-27.88	10.90	1.20
Bistatic Angle (°)	Vertical Polarisation			
	Mono		Bi	
	Sigma (Hz)	CoG (Hz)	Sigma (Hz)	CoG (Hz)
60	12.46	-9.31	12.32	5.54
90	11.68	-11.48	15.62	2.70
120	11.89	-16.00	10.90	2.12

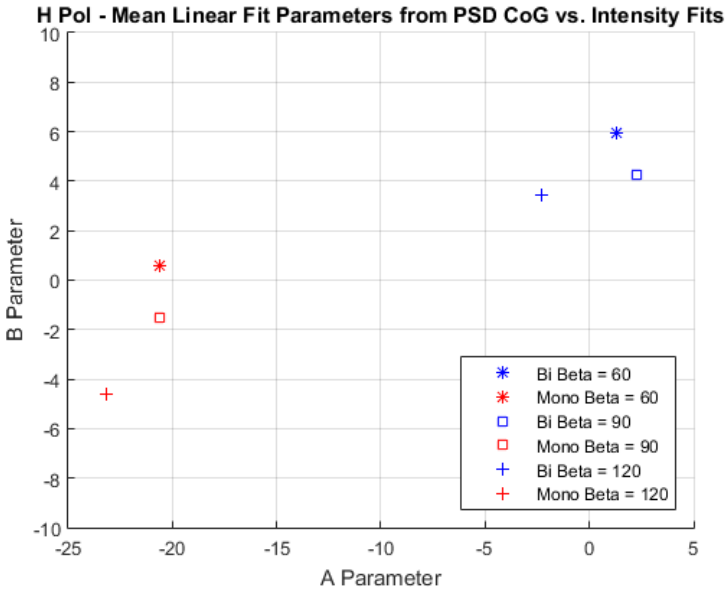

Figure 9 H Pol - Monostatic and Bistatic Linear fit parameter A vs. B

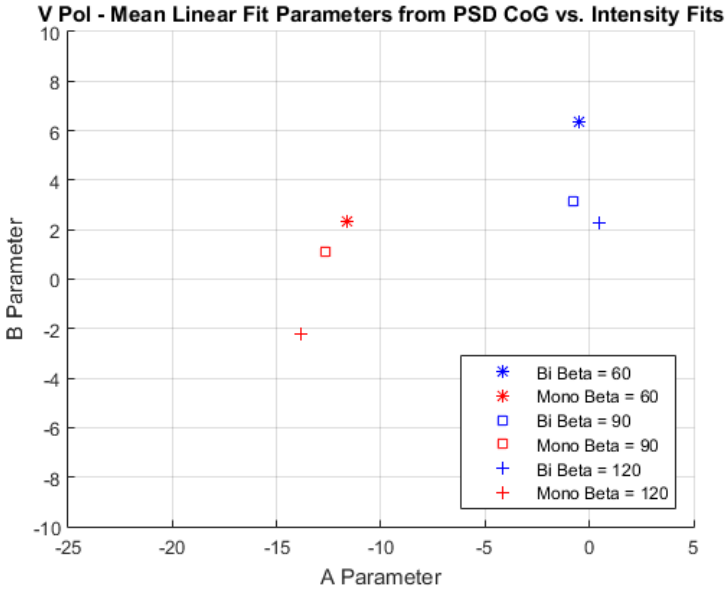

Figure 10 V Pol - Monostatic and Bistatic Linear fit parameter A vs. B

Table 6 Averaged CNR from time series data over range gates of interest

Bistatic Angle (°)	H CNR (dB)		V CNR (dB)	
	Mono	Bi	Mono	Bi
60	8.9	6.1	19.7	9.9
90	13.4	9.5	22	12.6
120	13.9	14.3	24	23.8

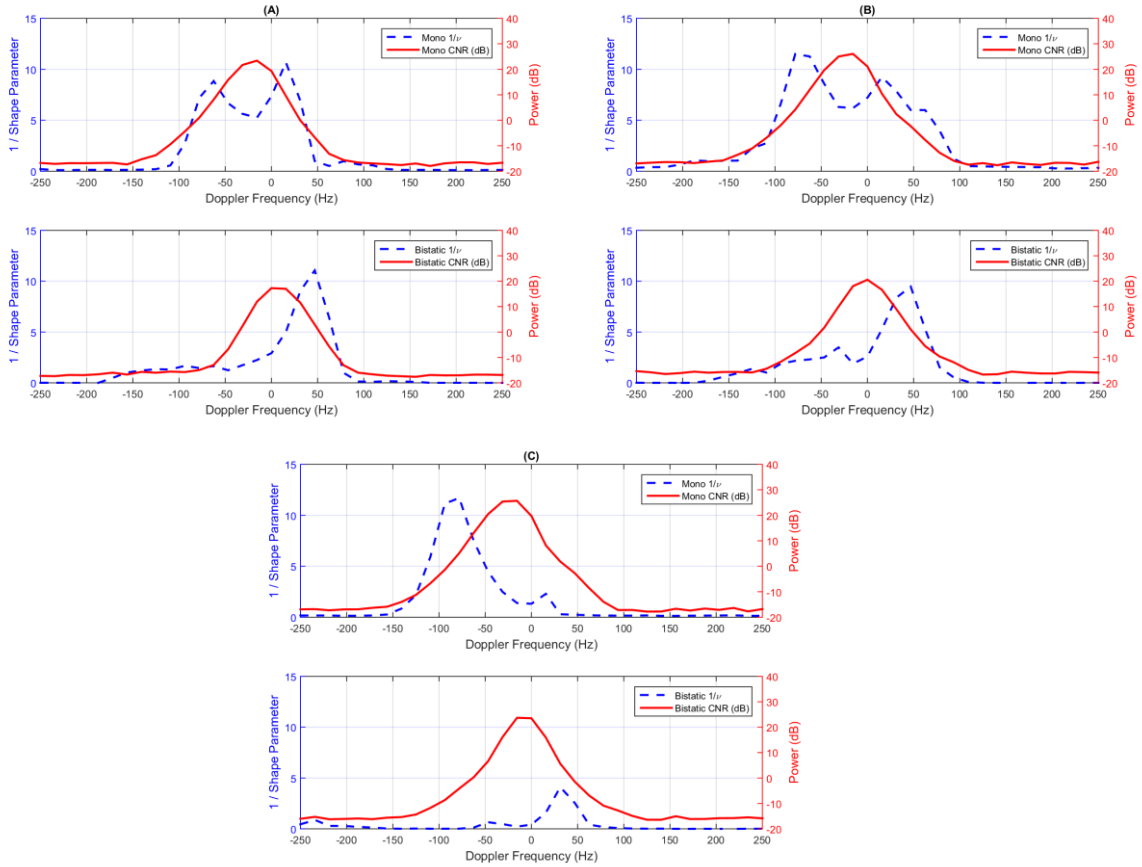

Figure 11 H pol – Average Inverse Shape Parameter vs. Doppler Frequency (Hz) (a) β = 60°, (b) β = 90°, (c) β = 120° upper is monostatic and lower is bistatic data

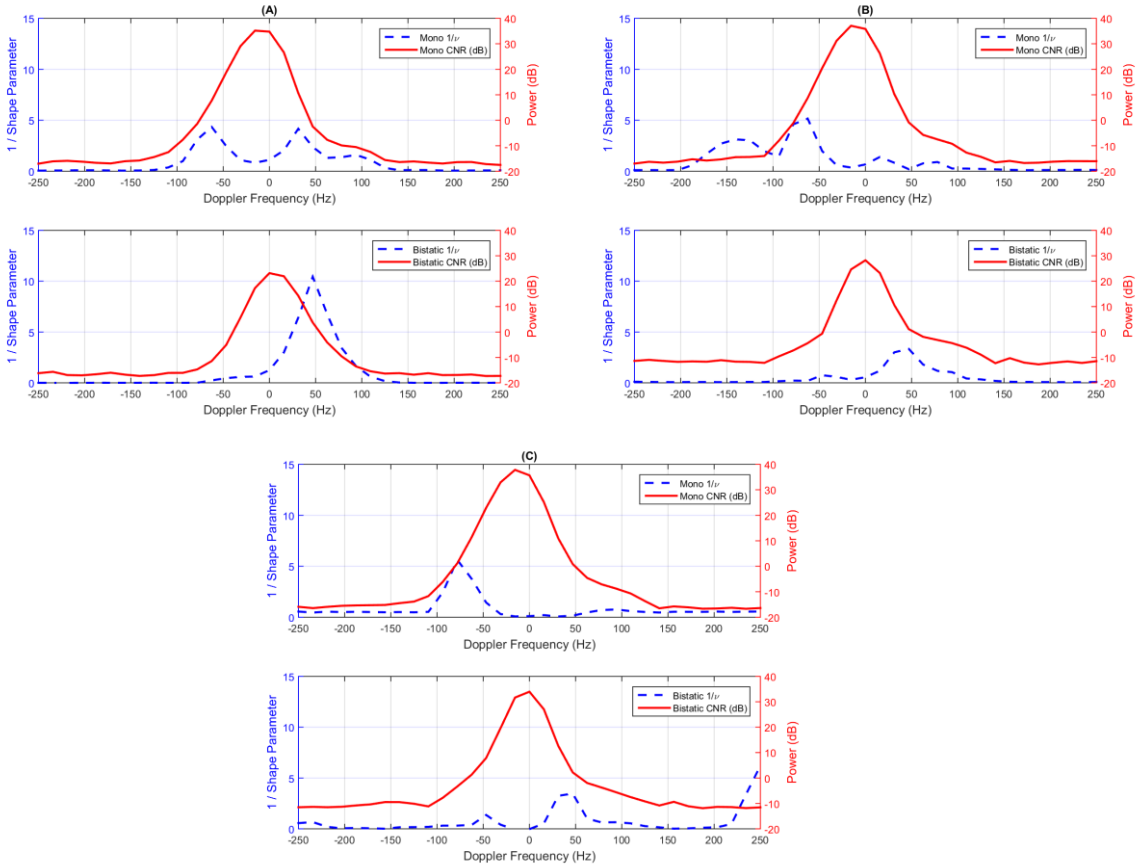

Figure 12 V pol – Inverse Shape parameter vs. Doppler Frequency (Hz) (a) β = 60°, (b) β = 90°, (c) β = 120° upper is monostatic and lower is bistatic data